Modelling of CO_2 circulation in the Colli Albani area

M. TODESCO[1]* & G. GIORDANO[2]

[1]*Istituto Nazionale di Geofisica e Vulcanologia, Sezione di Bologna, Via Donato Creti, 12, 40127, Bologna, Italy*

[2]*Dipartimento di Scienze Geologiche, Università degli Studi di Roma Tre, Largo S. Leonardo Murialdo, 1, 00146, Roma, Italy*

**Corresponding author (e-mail: todesco@bo.ingv.it)*

Abstract: The Colli Albani is a quiescent volcano located near the city of Roma, characterized by the presence of an active geothermal system, periodic seismic swarms and intense diffuse degassing. Several accidents, some lethal, have occurred in recent years associated with episodes of more intense releases and outbursts of volcanic gases, predominantly CO_2 and H_2S. Gas emissions presently comprise the most hazardous phenomenon for the highly populated Colli Albani area, and there is always the potential for the occurrence of seismic activity. This chapter presents numerical modelling of heat and fluid circulation, applied to study the mechanisms that control the diffuse degassing at Colli Albani volcano. Multi-phase and multi-component simulations were carried out using the TOUGH2 geothermal simulator in a realistic geological context, which includes all available information on the stratigraphy and structure of the Colli Albani substrate, together with data on the total gas flux, the local geothermal gradient, the local hydrogeology and the thermal characteristics of the rocks. The geothermal reservoir at Colli Albani is hosted by the 2000–3000-m-thick Mesozoic–Cenozoic carbonatic succession, capped by Pliocene clays that act as an aquiclude and are few hundreds to over 1000 m thick, which are in turn covered by continental sedimentary and volcanic deposits that host the shallow hydrogeological system. Numerical simulations evaluate the effects associated with the thickness of the carbonatic basement and its cap rock, the role of CO_2 supply rate at depth, and the influence of permeable channel-ways through the cap rocks. Numerical simulations show that the thickness of the geothermal reservoir hosted by the carbonatic basement and of its impervious cover control the vigour of the convection, the extent and depth (and hence temperature) of the lateral recharge area, and the distribution of the CO_2 within the system. This result suggests that the temperature distribution and diffuse degassing at the surface reflect not only the characteristics of the heat and fluid source at depth, but also the specific structure and hydrological properties of the site where they are measured.

The Colli Albani volcano is a Quaternary volcanic field located near the city of Roma (Fig. 1). No eruptions have taken place during historical times, but the volcano has recently been reclassified as quiescent based on documented Holocenic phreatic activity associated with the Albano maar lake (Funiciello *et al.* 2003; De Benedetti *et al.* 2008). In recent times, its state of activity has been characterized by periodic seismic swarms and ground deformation (Amato *et al.* 1994; Amato & Chiarabba 1995; Chiarabba *et al.* 1997). Diffuse degassing is also common in the area and, at some locations, can be a significant health hazard (cf. Chiodini & Frondini 2001; Carapezza *et al.* 2003, 2010; Cioni *et al.* 2003; Carapezza & Tarchini 2007; Barberi *et al.* 2007; Voltaggio & Spadoni 2009). Gas emissions mostly consist of CO_2, which is abundant in the groundwater, but H_2S, N_2, and CH_4 are all present in variable amounts. Rn activity is also very high in the zones where CO_2 emission occurs. The isotopic composition of carbon and the relatively high $^3He/^4He$ ratio (0.68–1.46) indicate a deep origin, associated with magma or mantle degassing and with metamorphic reactions. Measurements of diffuse CO_2 degassing have been carried out at different locations (Fig. 1; Chiodini & Frondini 2001; Beaubien *et al.* 2003; Carapezza *et al.* 2003). At Cava dei Selci a total amount of 95.7 ton/day has been measured over an area of 12 000 m^2, corresponding to *c.* 9×10^{-5} kg m^{-2} s^{-1}. Other areas of significant gas release are La Zolforata (1×10^{-5} kg m^{-2} s^{-1}) and Vigna Fiorita, where the removal of the impervious lahar cover led to CO_2 flux up to 6×10^{-4} kg m^{-2} s^{-1}. Gambardella *et al.* (2004) performed a detailed analysis of the CO_2 flows in central Italy, and identified a deep carbon component for the Colli Albani volcanic district that was quantified as 2.54×10^6 mol km^{-2} a^{-1}, corresponding to 3.54×10^{-10} kg m^{-2} s^{-1}.

Geochemical data indicate the presence of a pressurized, CO_2-rich gas reservoir, probably

From: FUNICIELLO, R. & GIORDANO, G. (eds) *The Colli Albani Volcano*. Special Publications of IAVCEI, **3**, 311–329. Geological Society, London. 1750-8207/10/$15.00 © IAVCEI 2010.

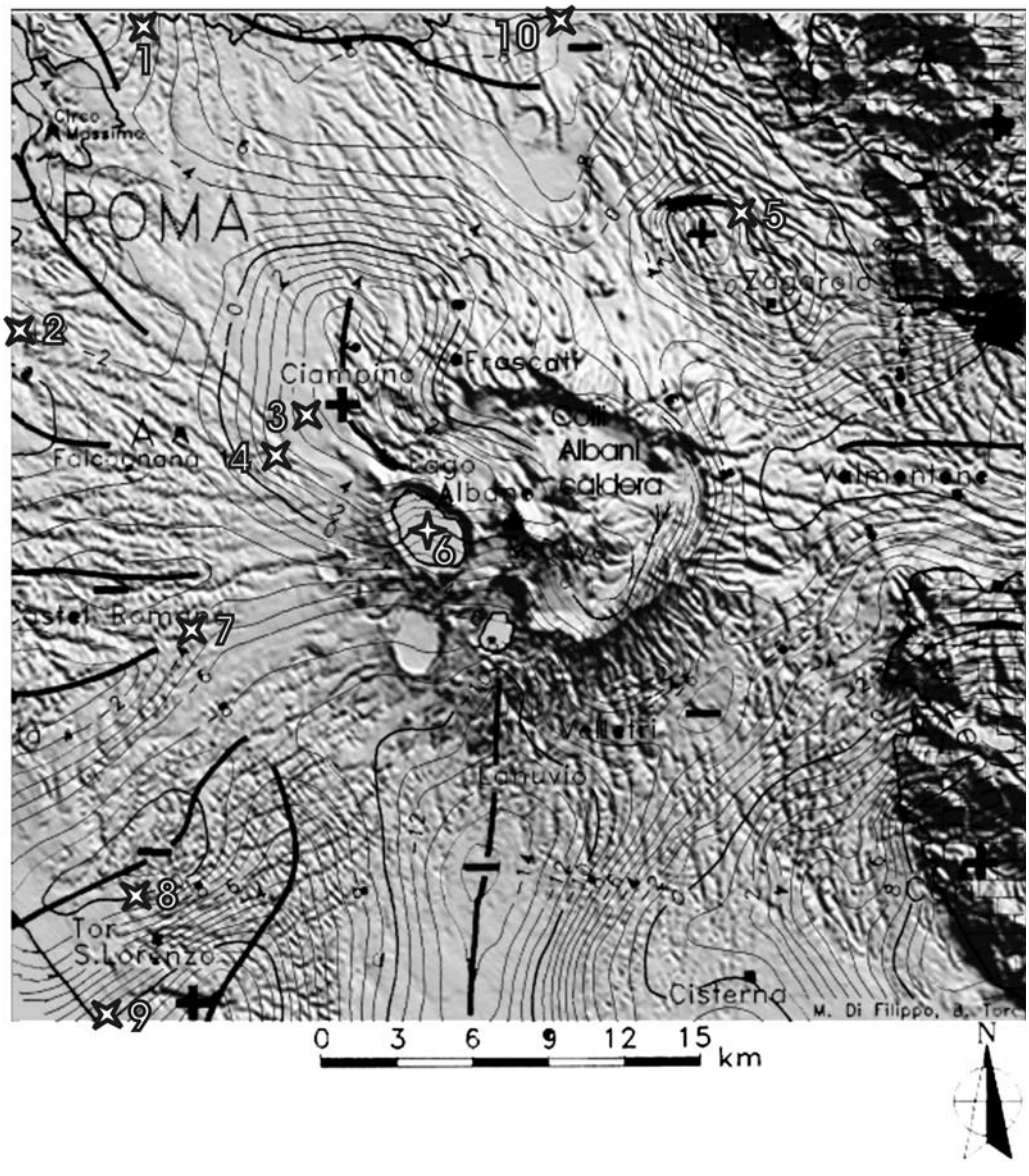

Fig. 1. Digital Elevation Model (DEM) of the Colli Albani volcano and the regional Bouguer gravimetry (from Di Filippo & Toro 1995). The stars highlight sites where high diffuse degassing has been measured: 1, Acquacetosa; 2, Acqua S. Paolo (Laurentina); 3, Cava dei Selci; 4, S. Maria delle Mole; 5, Fosso dell'Acqua Rossa; 6, Albano Lake; 7, La Zolforata; 8, Ardea; 9, Tor Caldara; 10, Tivoli (modified from Giordano *et al.* 2006).

hosted in the aquifers beneath and within the volcanic cover. The accidental burst of a shallow geothermal well in 1986 and again during the drilling of some water wells (Carapezza & Tarchini 2007; Barberi *et al.* 2007) corroborate the existence of such a pressurized system. Sudden releases of CO_2 and rapid heating of water springs have also been reported in relation to seismic events (Funiciello *et al.* 2003; Tuccimei *et al.* 2006).

Emissions are also present near and within the Albano lake, where volcanic gases percolate through the lake bottom and dissolve into the lake waters at depth (Anzidei *et al.* 2008). CO_2 storage in the lake's water is associated with a potential

(although not impending) hazard, as testified by the presence of lahar deposits related to lake overflows (cf. Tavolato Formation; Funiciello *et al.* 2003; De Benedetti *et al.* 2008; Giordano & The CARG Team 2010). In this work, numerical modelling of heat and fluid circulation has been applied to study the mechanisms controlling diffuse gas emissions at the Colli Albani volcano. Simulations were carried out to evaluate conditions favouring the ascent and exsolution of CO_2 from the carbonatic basement up to the shallow volcanic series hosting the water table. Numerical simulations evaluate the effects associated with the thickness of the carbonatic basement and its cap rock, the role of CO_2 supply rate at depth, and the influence of permeable channel-ways through the cap rocks (Table 1). The resulting reservoir conditions and degassing rate at the surface are compared for the different cases.

Preliminary results show that overall fluid circulation and surface CO_2 emissions are highly affected by the thickness and physical properties of the carbonatic basement, which acts as the main geothermal reservoir.

The geological-hydrogeological framework

The ascent and propagation of deep-seated gases is controlled by the rate at which they are generated at depth, but they also depend on the hydrogeological properties of the rocks through which they flow. The reconstruction of the Colli Albani geology is described in the chapters by Mattei *et al.* and Giordano & The CARG Team 2010 (cf. Giordano *et al.* 2006; Bianchi *et al.* 2008), whereas the hydrogeology is described by the chapter by Mazza & Capelli 2010 (cf. Boni *et al.* 1995; Capelli *et al.* 2006). The permeable volcanic edifice overlies a regional aquiclude, several hundreds of metres thick, composed of alternating marine clay and sand belonging to the Pliocene–Quaternary post-orogenic succession. This formation represents the main cap rock. A highly permeable Meso–Cenozoic carbonatic succession forms the basement and the main geothermal reservoir for the area (Chiodini & Frondini 2001; Gambardella *et al.* 2004; Carapezza & Tarchini 2007) (Fig. 2). This basement is affected by syn-orogenic thrust tectonics and post-orogenic extensional tectonics forming structural highs and lows (Fig. 2) that are clearly identified from gravity data (Fig. 1; Di Filippo & Toro 1995; Mattei *et al.* 2010). Gas emissions are usually associated with structural highs that act as traps, and with local tectonic discontinuities that represent preferential pathways for fluid ascent. The geothermal system is sustained by the Colli Albani magma chamber, which is located largely below and partly within the carbonatic series (cf. Conticelli *et al.* 2010).

Table 1. *Performed numerical simulations*

Simulation	Feeding rate (kg m^{-2} s^{-1})	Structural settings	Impervious layers
1	10^{-9}	High	Continuous
2	10^{-9}	Low	Continuous
3	10^{-7}	High	Continuous
4	10^{-7}	Low	Continuous
5	10^{-9}	High	Gap through Pisolitic Tuffs
6	10^{-9}	Low	Gap through Pisolitic Tuffs
7	10^{-9}	High	Gap through clay
8	10^{-9}	Low	Gap through clay

Numerical model and computational domain

Fluid circulation at Colli Albani was simulated with the TOUGH2 geothermal simulator (Pruess *et al.* 1999). This multi-phase and multi-component model describes the coupled flow of heat and fluids through heterogeneous porous media. In the present application, the considered fluid components are water and CO_2. The model accounts for the dissolution of CO_2 in liquid water according to Henry's law, and describes water phase change as a function of system conditions.

All the geological, geophysical, geochemical and hydrogeological information available for the Colli Albani region have been considered to provide a reliable description of the underground rock sequence, with the most relevant porous domains. Physical and hydraulic properties assigned to each rock unit are reported in Table 2. Two schematic stratigraphic sequences were defined to represent typical conditions of structural high and low (Fig. 3).

The computational domain and boundary conditions are shown in Figure 4. The domain is initially cold and water saturated. Heat (0.1 W m^{-2}) and hot (*c.* 350 °C) CO_2 (10^{-9} kg m^{-2} s^{-1}) are injected along the base of the domain until the steady state is reached, for each of the two considered rock sequences (simulations 1 and 2). Heating and fluid flow prompt a vigorous convection within the permeable carbonatic basement for both structural settings (Fig. 5). At steady state, a wide, clockwise convective cell occupies the entire basement, but negligible fluid motion occurs at shallower depths (Fig. 5b, d). The CO_2 released at the bottom dissolves in the water, rises along the symmetry axis,

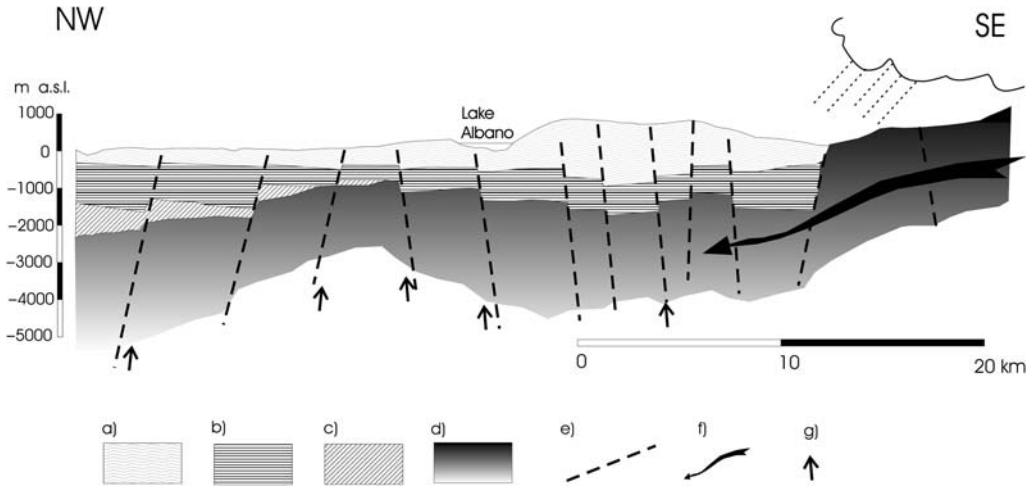

Fig. 2. Geologic section through the Colli Albani volcano with structural high and lows (modified from Duchi *et al.* 1991). a, Volcanic and sedimentary Quaternary deposits; b, Pliocene marine clay; c, Liguride flysch; d, Mesozoic–Cenozoic carbonatic succession; e, faults; f, groundwater recharge; g, CO_2 and geothermal fluids upflow paths.

and accumulates at the base of the low-permeability clay layer. Hot water propagates outwards, along the base of the clay, and finally leaves the domain through its outer boundary, 10 km from the symmetry axis. Recharge of cold, liquid water occurs through the same vertical boundary at greater depths. With time, CO_2 penetrates within the clay layer and slowly propagates, forming a wide plume. Eventually, in both simulations, some minor fractions of CO_2 (0.06) exsolve to form a water-dominated two-phase region, delimited by the thick, black line in Figure 5b, d. Diffuse degassing takes place where the gas phase develops, as shown in Figure 5a, c. Although the evolution in the two considered cases is qualitatively similar, the different geometries associated with the structural high and structural low cause some significant differences. The thinner basement in simulation 2 prompts a more vigorous convection. CO_2 is more effectively diluted and reaches a lower concentration within the plume. The thicker clay layer hinders the ascent of CO_2 towards the surface, and the resulting degassing rate does not exceed 0.2×10^{-9} kg m^{-2} s^{-1}. In contrast, CO_2 concentrates in the case of a structural high, and achieves higher partial pressures (up to 5 MPa at the steady state) (Fig. 5b). The higher CO_2 enrichment in turn leads to the development of a wider two-phase zone and stronger degassing rate at the surface (up to 0.8×10^{-9} kg m^{-2} s^{-1}). The structural setting also affects the temperature distribution within the system at the steady state (Fig. 6). In both the considered cases, the shallow layers above the impermeable clay are heated mostly by conduction, and remain colder, whereas the permeable basement is effectively heated by convection. In the case of a structural high, convection carries heat over a wider portion of the domain and, at the same time, the outer boundary is permeable over a larger fraction of its length, allowing an effective recharge of cold water. As a result, temperatures in excess of 150 °C are found at depths shallower than 1000 m,

Table 2. *Rock properties considered in the numerical simulations*

Rock type	Density (kg m^{-3})	Porosity	Permeability (m^2)	Heat conductivity (W m^{-1} K^{-1})	Specific heat (J kg^{-1} K^{-1})
Volcanics	2000	0.45	10^{-12}	0.8	900
Pisolitic Tuffs	1500	0.35	10^{-15}	0.8	900
Sand	2300	0.25	10^{-14}	2.0	1000
Clay	1750	0.35	10^{-17}	1.5	1000
Carbonate	2800	0.1	10^{-12}–10^{-14}	1.1	900

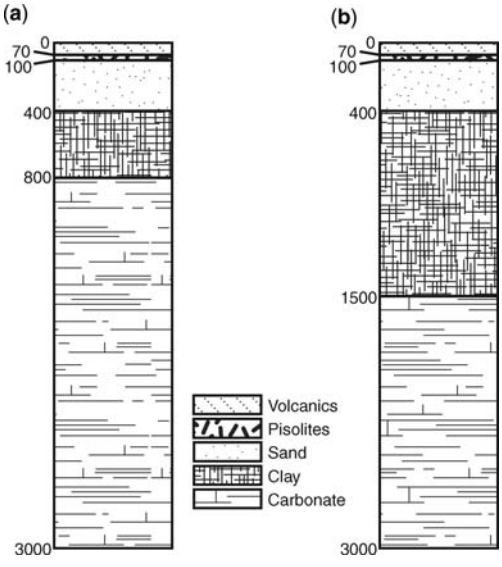

Fig. 3. Schematic sequence of rock types implemented to represent a structural high (**a**) and low (**b**) in the simulations. Different lithologies, characteristic of the area, are listed in the legend. Numbers refer to depth (m) below sea level.

but are never exceeded (Fig. 5a). In the case of a structural low, higher maximum temperatures are achieved (200 °C), but are confined to greater depths, within the carbonatic basement. A more uniform and effective heating is ensured by the thicker cap rock, the more vigorous convection, and the smaller recharge area along the outer boundary (Fig. 5b).

Steady-state conditions can also be examined in terms of vertical profiles of selected variables.

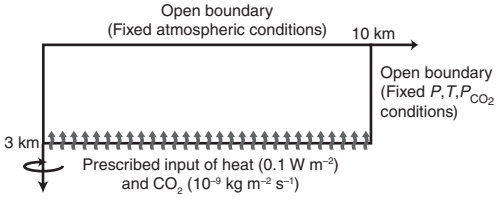

Fig. 4. Two-dimensional, axisymmetric computational domain and boundary conditions. The computational grid is composed of 1534 elements with radial dimensions ranging from 50 to 1500 m and vertical dimensions from 10 to 200 m. Fixed values of the primary variables are assigned along the open boundaries, and correspond to atmospheric pressure and temperature along the top, and to the initial pressure and temperature distribution along the vertical boundary. Prescribed heat and CO_2 flows are imposed along the bottom.

Figure 7 shows the distribution of CO_2 partial pressure, temperature and gas fraction with depth, along the symmetry axis. A comparison of the profiles associated with the two structural settings clearly shows how the same boundary conditions result in a different distribution of the variables at the steady state. The structural high (dashed line) is characterized by higher values of CO_2 partial pressure and of gas saturation at all depths. The temperature profiles clearly identify the deep, isothermal region dominated by convection, and the shallow conductive layers, characterized by a strong thermal gradient, for both cases considered. The structural high is hotter from the surface to the base of the clay layer, with a lower temperature within the basement. A thicker two-phase region is present in the case of the structural high, but the maximum gas saturation is similar in the two cases, and always very low (0.06).

System perturbations

Starting from the steady system conditions described above, some perturbations were imposed to evaluate their effects on phase distribution and surface degassing.

The fluid source at depth

The first perturbation is related to the rate of CO_2 generation at depth (simulations 3 and 4). A stronger CO_2 injection rate (10^{-7} kg m^{-2} s^{-1}) is imposed near the symmetry axis to represent a localized inlet (100 m wide) of magmatic volatiles (Fig. 8a). The gas flow rate along the rest of the bottom boundary remains unchanged (10^{-9} kg m^{-2} s^{-1}). Heat flow is fixed at 0.1 W m^{-2} along the entire boundary, as in simulations 1 and 2. The same boundary conditions shown in Figure 4 are applied once again to both the considered structural domains.

Figure 9 illustrates the temporal evolution of the CO_2 partial pressure in the case of a structural high (Fig. 9a–c) and a structural low (Fig. 9d–f). In both cases, the system evolution is very slow, despite the high permeability assigned to the carbonatic basement. The larger CO_2 injection at the inlet (white arrows on the bottom axes) progressively increases the amount of CO_2 that propagates along the symmetry axis. After 10 000 years, and for the structural high (Fig. 9a), most of the gas accumulates within the permeable basement, whereas minor amounts propagate through the low-permeability clay layer. At this time, some fraction (0.036) of gas (thick, black line) develops under the clay (at −800 m depth) near the symmetry axis. As the slow propagation through the shallow layers proceeds, the amount of gas increases progressively. At the

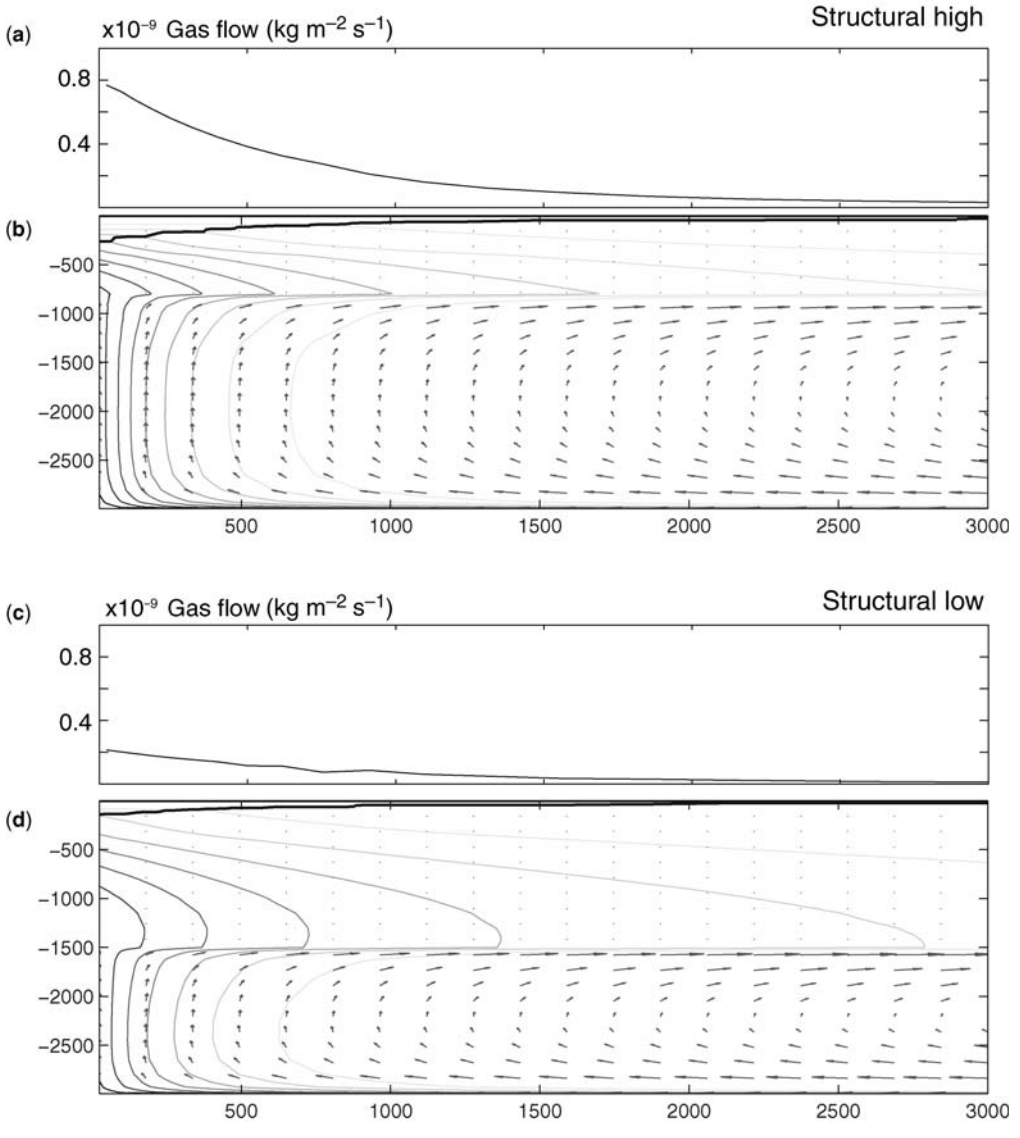

Fig. 5. Steady-state conditions for simulations 1 and 2. Gas flow rate (kg m^{-2} s^{-1}) along the surface (**a**, **c**) and distribution of CO_2 partial pressure (MPa) (**b**, **d**) for the cases of a structural high (a, b) and low (c, d). Vectors highlight the pattern of liquid flow. Contour lines represent every 0.5 MPa, from 1 to 5 MPa. The thick black line indicates the extent of the two phase zone. These conditions are taken as initial conditions for the following simulations.

steady state (*c*. 1 Ma, Fig. 9c), a funnel-shaped two-phase zone has developed from the surface down to a maximum depth of *c*. 900 m (black line), with a maximum gas fraction of *c*. 0.09. The CO_2 partial pressure within the shallow clay layer has reached *c*. 8 MPa.

The evolution in the case of a structural low is qualitatively similar (Fig. 9d–f). The CO_2 rises along the symmetry axis and spreads out along the base of the clay. The higher pore pressure at this depth prevents the development of a gas phase at the base of the clay. A slow propagation takes place through the clay layer, where the CO_2 partial pressure is as high as 7 MPa at the steady state. Gas exsolution at shallower depths contributes to increasing the size of the two-phase zone, which, in this case, reaches but does not penetrate the top of the clay layer, at a depth of 400 m.

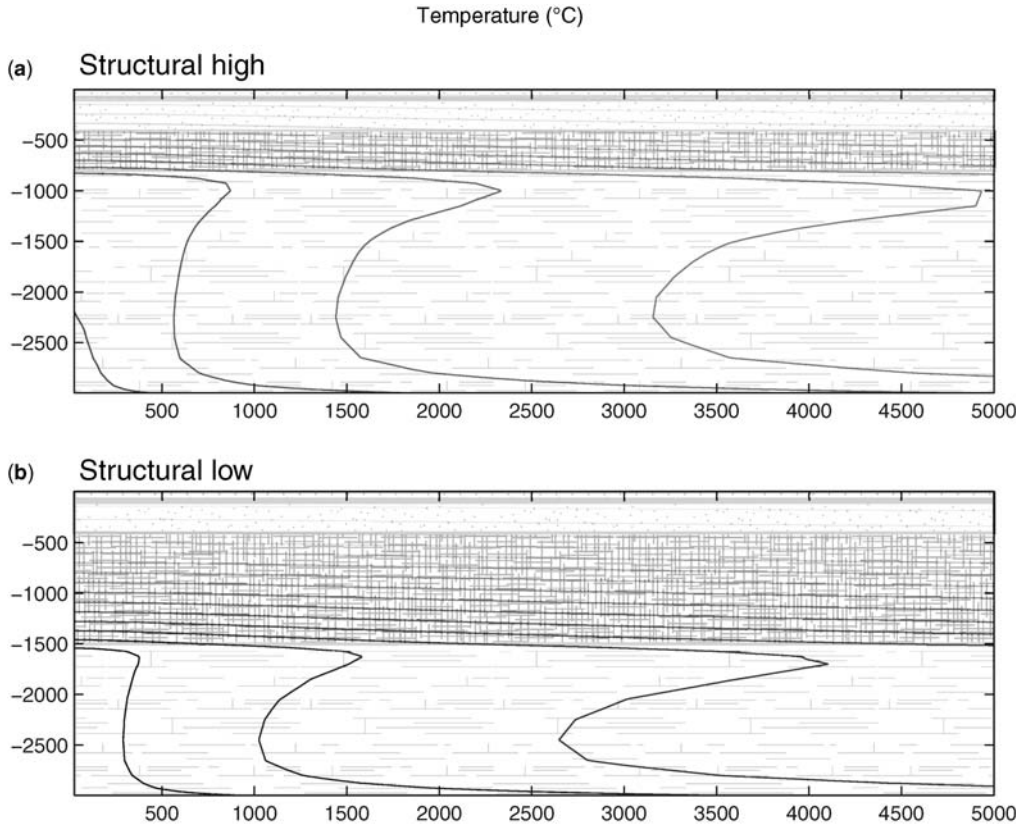

Fig. 6. Steady-state conditions for simulations 1 and 2: temperature (°C) distribution for structural high (**a**) and low (**b**). Contour lines at every 10 °C, from 30 to 180 °C. Steady-state conditions are taken as initial conditions for the following simulations. Different patterns indicate lithologies, as shown in Figure 3.

The stronger activity of the CO_2 source at depth increases the overall amount of gas within the system. It is interesting to observe how the properties of the shallow layers affect the distribution of the gas phase, which tends to concentrate within the less permeable strata (Fig. 10). This behaviour is associated with the mobility of the two phases, which in turn depends on their saturation. As the gas phase occupies only a minor fraction of the pore volume (its saturation is always below 0.1), its mobility is reduced by the pervasive presence of liquid water. For this reason, once the gas reaches a low-permeability layer, it tends to become immobile and it accumulates, as new gas ascends from below.

The stronger CO_2 source affects the variables distribution and degassing rate at the steady state (Fig. 11). The CO_2 partial pressure along the symmetry axis (Fig. 11a) increases at all depths, for both structural settings, but the temperature profiles (Fig. 11b) are not affected by the stronger activity of the source. The volumetric gas fraction undergoes major changes, especially in the case of a structural high, where gas saturation reaches larger values over a wider range of depths (Fig. 11c). Maximum values of gas saturation highlight the presence of less permeable layers in both simulations. The increment in gas fraction is also associated with a higher degassing rate at the surface, up to 1.1×10^{-9} kg m^{-2} s^{-1} in the case of a structural high (Fig. 11d). The effect of the source at depth is mostly confined to the axial region, above the location of the 'magmatic' source.

Opening through the impervious layers

Further simulations were run to evaluate the effects of a discontinuity of the impervious layers. In the first case (simulations 5 and 6), the shallow Pisolitic Tuff layer is interrupted near the symmetry axis (Fig. 8b), whereas in the second case (simulations 7 and 8), the gap affects the thicker and deeper

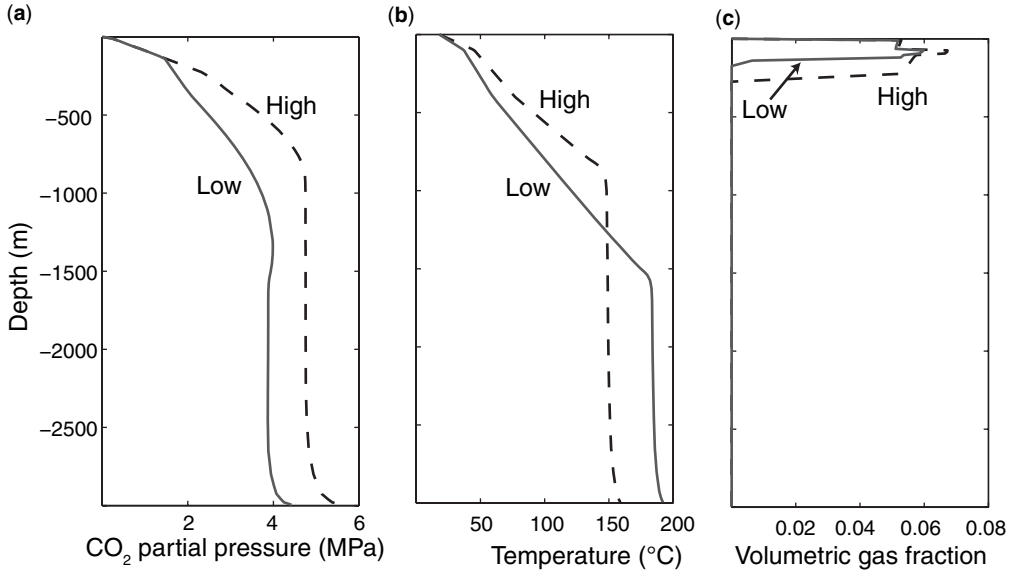

Fig. 7. Simulations 1 and 2. Distribution of CO_2 partial pressure (**a**, MPa), temperature (**b**, °C), and volumetric gas fraction (**c**) v. depth, along the symmetry axis. Dashed line, structural high; solid line, structural low.

clay layer (Fig. 8c). These gaps could be due to a non-uniform sedimentation, or to a fault or fracture zone.

Simulation 5 refers to the case in which the shallow Pisolitic layer is interrupted and the rock sequence corresponds to a structural high. Initial conditions are taken from the steady state achieved in simulation 1. The presence of the gap influences the circulation within the permeable, upper layer (Fig. 12a), and within 10 years, the faster fluid ascent through the gap drives a vigorous convection. This favours the circulation of cold, liquid water (available all along the upper boundary, which is water saturated and held at constant, atmospheric conditions). As a result, the two-phase zone is gradually disrupted within the upper layer. This evolution is reflected by the rate of diffuse degassing through the surface (Fig. 12b): initially, diffuse degassing is enhanced, as larger amounts of CO_2 propagate through the gap and reach the surface of the domain. With time, however, the liquid water permeates the shallow layer, hindering the gas ascent. At steady state (201 ka), surface degassing is absent near the symmetry axis. Steady-state conditions do not change significantly if the simulation is run from cold and CO_2-free initial conditions (i.e. if the gap existed since the deposition of the impermeable layer).

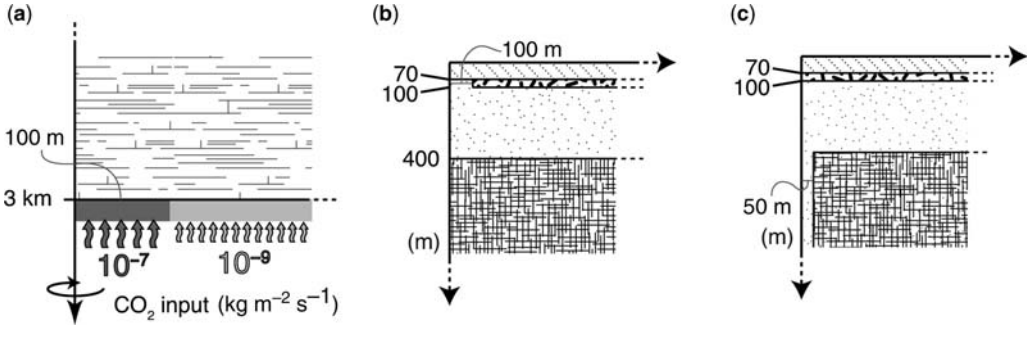

Fig. 8. Boundary conditions for simulations 3 to 8. (**a**) Size, flow rate and location of CO_2 sources along the bottom (simulations 3 and 4). (**b**) Size and position of the gap through the impermeable Pisolitc Tuff layer (simulations 5 and 6). (**c**) Size and position of the gap through the impermeable clay layer (simulations 7 and 8).

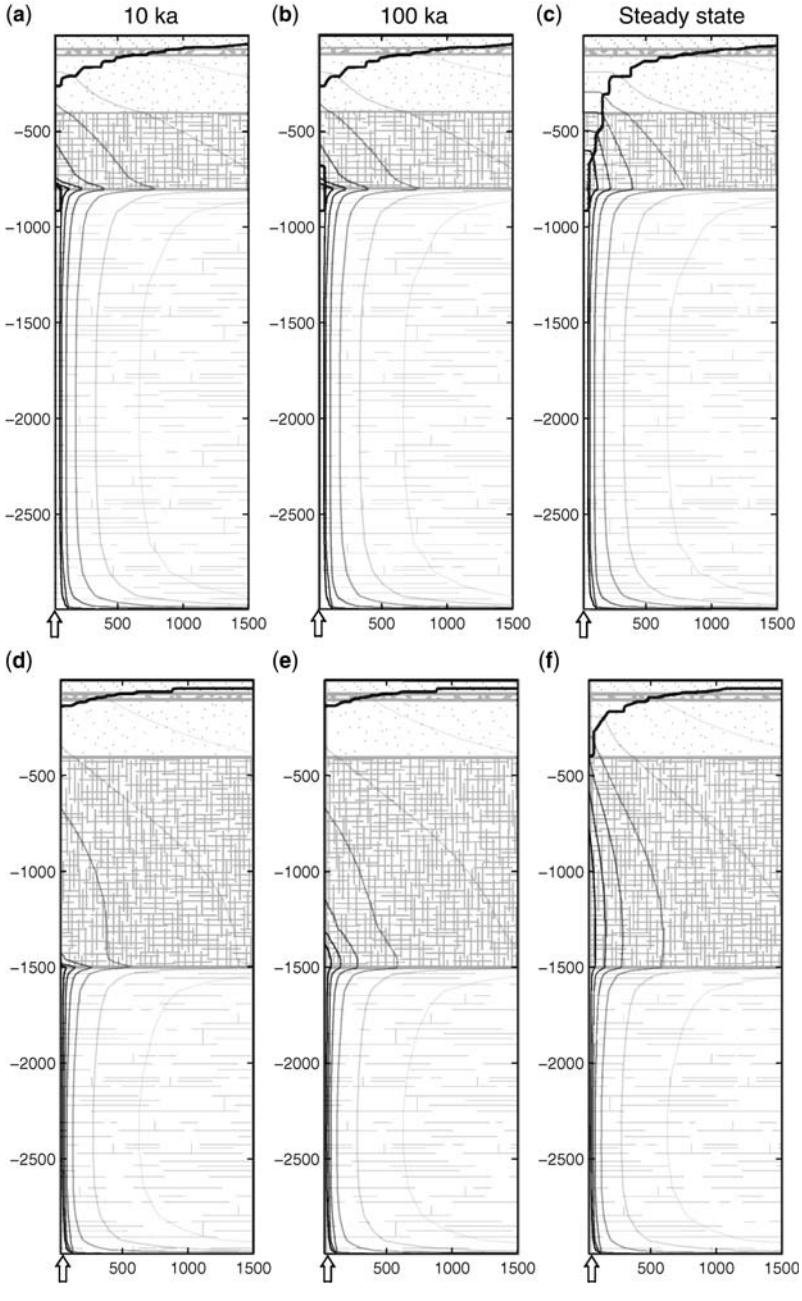

Fig. 9. Simulations 3 and 4. Distribution of CO_2 partial pressure at different times for a structural high (**a**, **b**, **c**) and low (**d**, **e**, **f**). Contour lines represent every 1 MPa, from 1 to 6 MPa. The thick black line indicates the extent of the two-phase zone. White arrows on the bottom axes indicate the position of the inlet of magmatic fluids. Different patterns indicate lithologies, as shown in Figure 3.

Although the fluid flow pattern changes significantly with respect to the initial conditions, these changes are confined to a very shallow depth and do not affect the overall temperature distribution within the system. The case of a structural low (simulation 6, not shown) is characterized by a similar evolution, with liquid water permeating the upper layer, and limiting surface degassing.

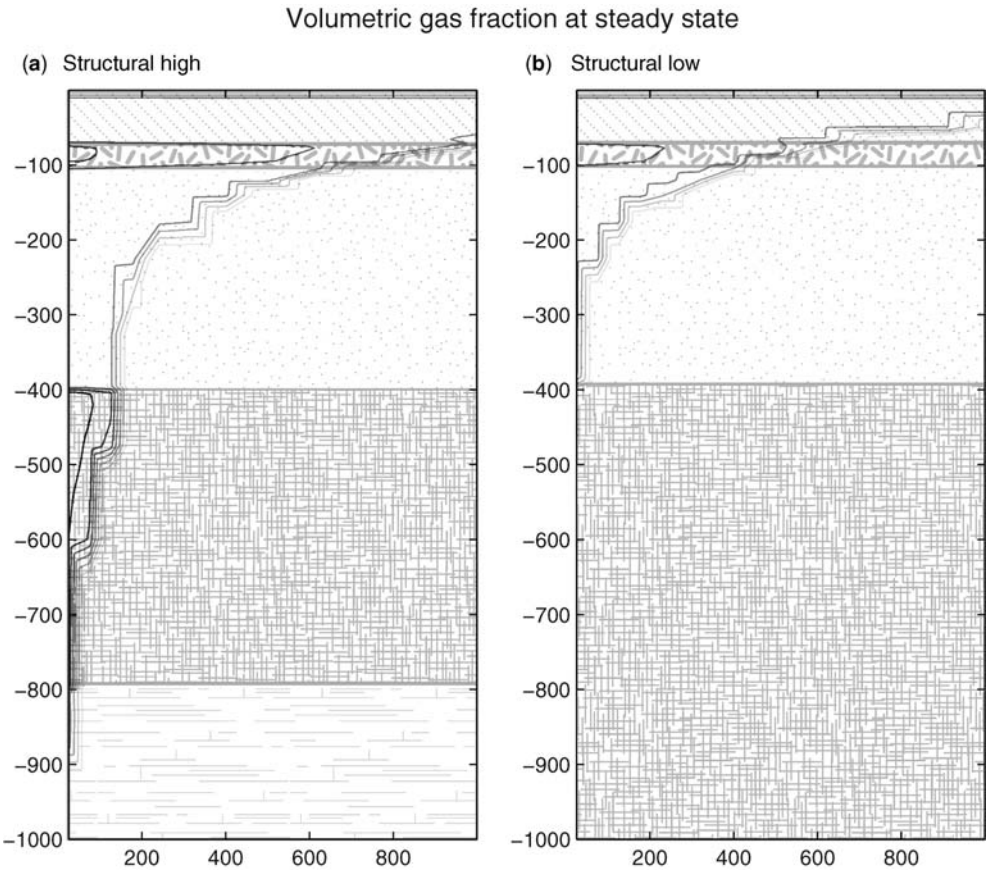

Fig. 10. Simulations 3 and 4. Distribution of volumetric gas fraction at the steady state in the case of a structural high (**a**) and low (**b**). Contour lines are plotted every 0.01 for gas fractions ranging from 0.02 to 0.08. Different patterns indicate lithologies, as shown in Figure 3.

The second set of simulations is performed with a gap affecting the impermeable clay layer at depth. Figure 13 illustrates the temporal evolution of the volumetric gas fraction for the case of a structural high (simulation 7). The thin vertical channel allows the ascent of deep-seated fluids, which add to the shallow two-phase region. CO_2 accumulates at the base of the Pisolitic Tuff layer (continuous, in this case) and, with time, affects the circulation within the upper layer as well. As a result, the two-phase region is once again partially disrupted at the steady state (994 ka, in this case). The ascent of deep-seated fluids modifies the temperature distribution within the system. Heating affects the entire permeable channel and temperatures in excess of 100 °C are found at depths of 400 m (Fig. 14a). Surface degassing increases significantly during the entire simulation. In particular, flow rates at the symmetry axis reach values as high as 6×10^{-8} kg m^{-2} s^{-1}.

In the case of a structural low (simulation 8), the evolution is similar, but lower amounts of gas reach the shallow two-phase region (Fig. 15a). This reflects on the circulation within the upper layer, where the two-phase region survives to steady state (553 ka). Fluid ascent is accompanied by heating, although slightly lower values are reached (Fig. 15b). Diffuse degassing increases throughout the simulation to a maximum value of 8×10^{-9} kg m^{-2} s^{-1}. Figure 16 illustrates the overall changes associated with the permeable channel: the two-phase region increases significantly for both settings, and the new pattern of circulation affects the overall distribution of CO_2. Heating at shallow depths is also evident from the vertical profile, and indicates the contribution of fluid flowing through the permeable channel.

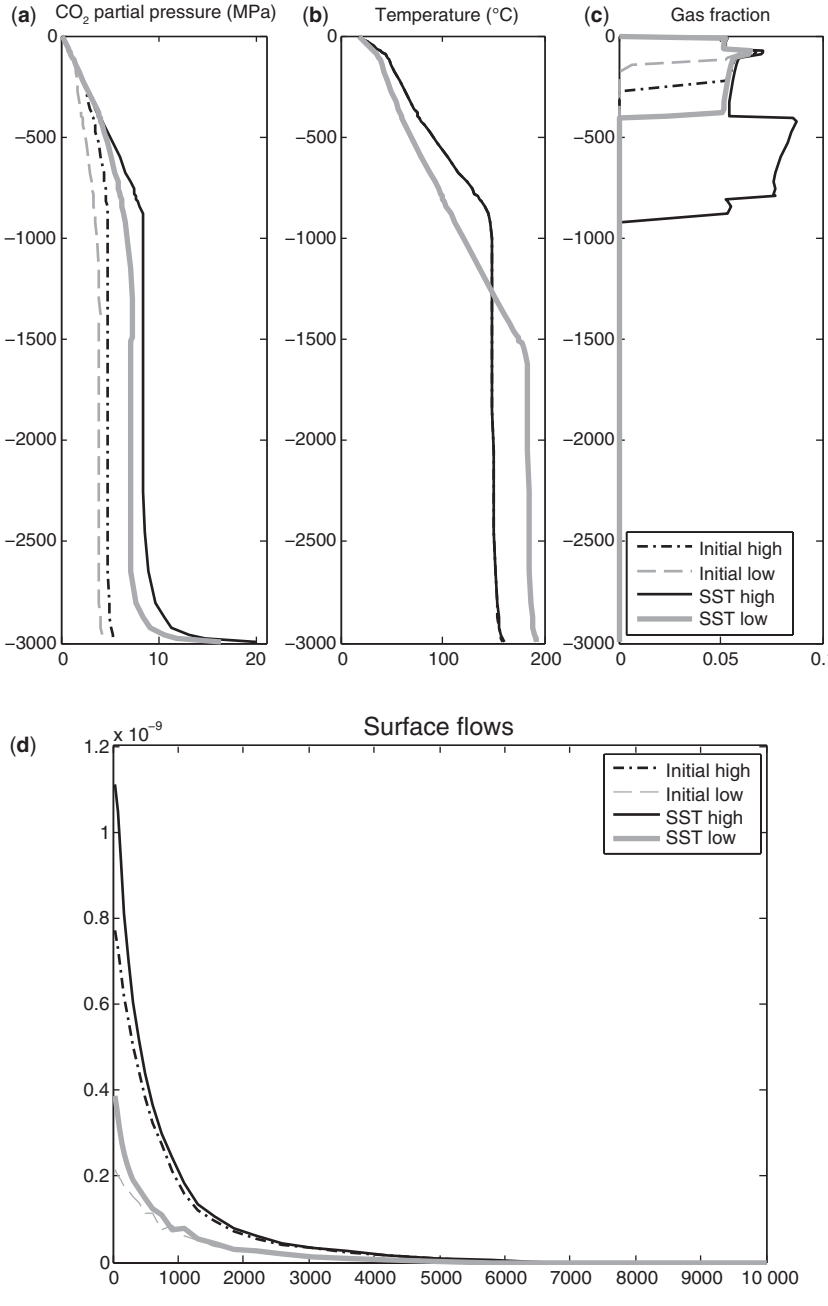

Fig. 11. Simulations 3 and 4. Distribution of CO_2 partial pressure (**a**, MPa), temperature (**b**, °C) and volumetric gas fraction (**c**) v. depth, along the symmetry axis, at the beginning of the simulations and at the steady state. (**d**) Gas flow rate along the surface at the beginning of the simulation and at steady state, for a structural high and low.

Discussion and conclusions

The Colli Albani volcano, although quiescent, has been the site of several accidents associated with CO_2 and H_2S degassing, some of which have been lethal (Carapezza *et al.* 2003, 2010; Carapezza & Tarchini 2007). The deep origin of the gases calls for a comprehensive conceptual model of the

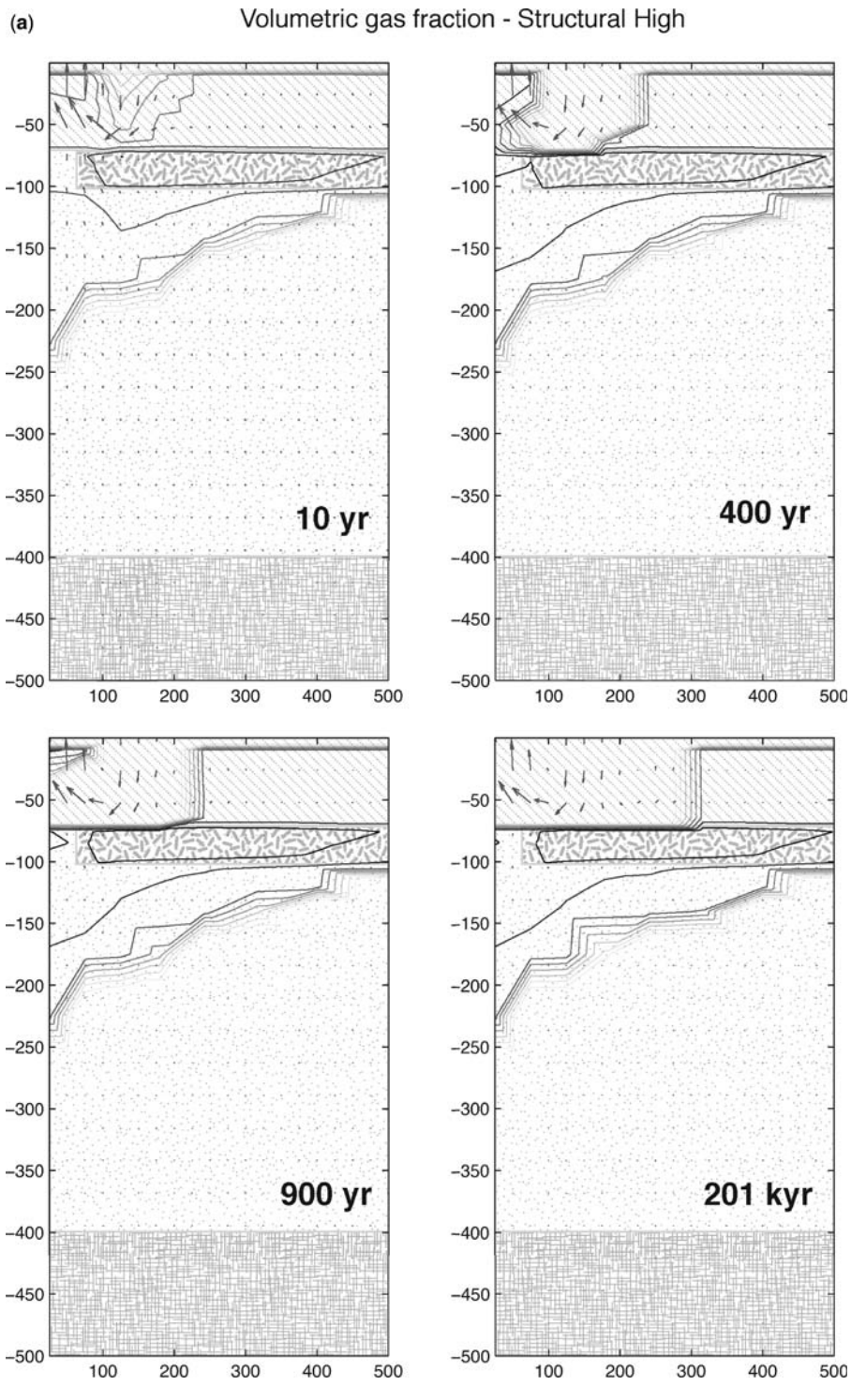

Fig. 12. Simulation 5. (**a**) Volumetric gas fraction and flow pattern of liquid water, at different times. Contour lines represent divisions of 0.005, from 0.02 to 0.065. The maximum flow rate of liquid water is 7.75×10^{-5} kg m^{-2} s^{-1}. Different patterns indicate lithologies, as shown in Figure 3, and highlight the gap through the shallow Pisolitic Tuff layer. (**b**) Gas flow rate along the surface at different times.

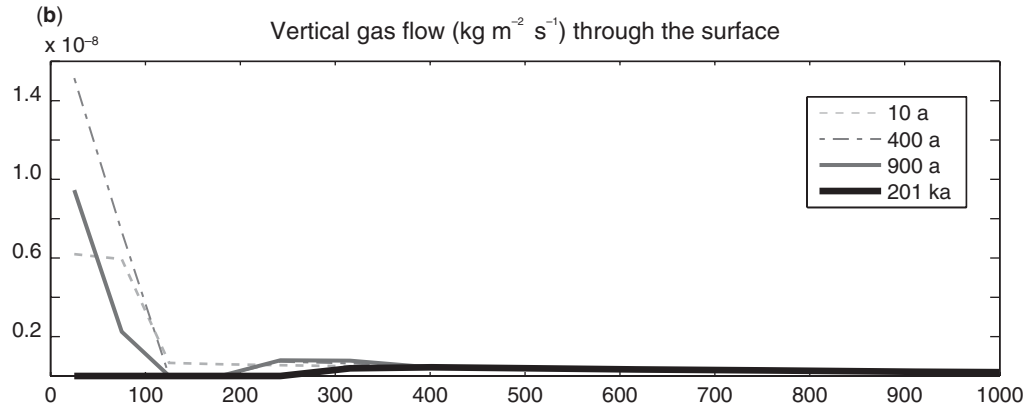

Fig. 12. (*Continued*)

geothermal field that underlies the volcano. However, early geothermal exploration at Colli Albani was dismissed after low temperatures (41 °C at 610 m depth) were detected in a deep well drilled in Falcognana in 1986 (ENEL 1990; see Danese & Mattei 2010). Low temperatures are consistent with the relatively low heat flow measured in the region, in contrast to the higher values characterizing the nearby high-enthalpy geothermal areas in Northern Latium (Mongelli *et al.* 1991). Other pieces of information derive from the observation of diffuse degassing and contribute to our current knowledge of the geothermal system. For example, it is widely acknowledged that diffuse degassing mostly occurs at structural highs (Fig. 1). CO_2 is known to exist as a free gas phase, at various depths below the impervious layers (Carapezza & Tarchini 2007; Barberi *et al.* 2007). Also, sudden releases of gas or hot fluids have been observed in association with local or distal earthquakes, although the relation between the two phenomena is not univocal.

The low temperatures and the common occurrence of diffuse degassing in the area have been traditionally explained assuming an efficient recharge of the aquifer within the carbonatic basement. Fresh water from the Apennines can quickly propagate through fast, karstic circuits and dilute the deep geothermal component (e.g. Giggenbach *et al.* 1988; Duchi *et al.* 1991; Chiodini & Frondini 2001). This interpretation is still mostly based on qualitative considerations. The first work aimed at a quantitative assessment of diffuse degassing at the scale of the volcano is still that by Chiodini & Frondini (2001), who interpolated data of CO_2 concentration in groundwater for the western, southern and central portion of the volcano. Based on those data, Gambardella *et al.* (2004) attempted a calculation of the total gas release from the volcano. Other works focused on limited areas of more intense degassing where accidents have occurred in the recent past, such as Cava dei Selci, La Zolforata and the Albano Lake (Annunziatellis *et al.* 2003; Beaubien *et al.* 2003; Carapezza *et al.* 2003, 2010; Barberi *et al.* 2007; Carapezza & Tarchini 2007).

Our work provides a first-order, quantitative framework to understand the Colli Albani geothermal/hydrogeological system and its relationship to diffuse degassing. A first result is related to the role of the structural setting of the area. Numerical simulations show that the thickness of the carbonatic basement and of its impervious cover control the vigour of the convection, the extent and depth (and hence temperature) of the lateral recharge area, and the distribution of the CO_2 within the system. Simulations relating to different structural settings end up with different geothermal gradients and degassing rates, even though boundary conditions are the same. In particular, the structural high is characterized by a lower temperature in the basement (*c.* 150 °C) and a steeper thermal gradient at shallower depths (Figs 6 & 7). CO_2 is efficiently conveyed towards the surface, and the resulting degassing rate is four times higher than that for a structural low (Fig. 5).

This result is relevant, because it suggests that data on the temperature distribution or diffuse degassing do not simply reflect the characteristics of the heat and fluid source at depth, but also the specific structure and hydrological properties of the site where they are measured. Our simulations are based on two ideal stratigraphic sequences that do not correspond to any specific location in the area. For this reason, we did not expect to match any specific data set. Nevertheless, the simulations confirm that structural highs are associated with stronger degassing (comparable with the estimates by Gambardella *et al.* (2004), and imply that low

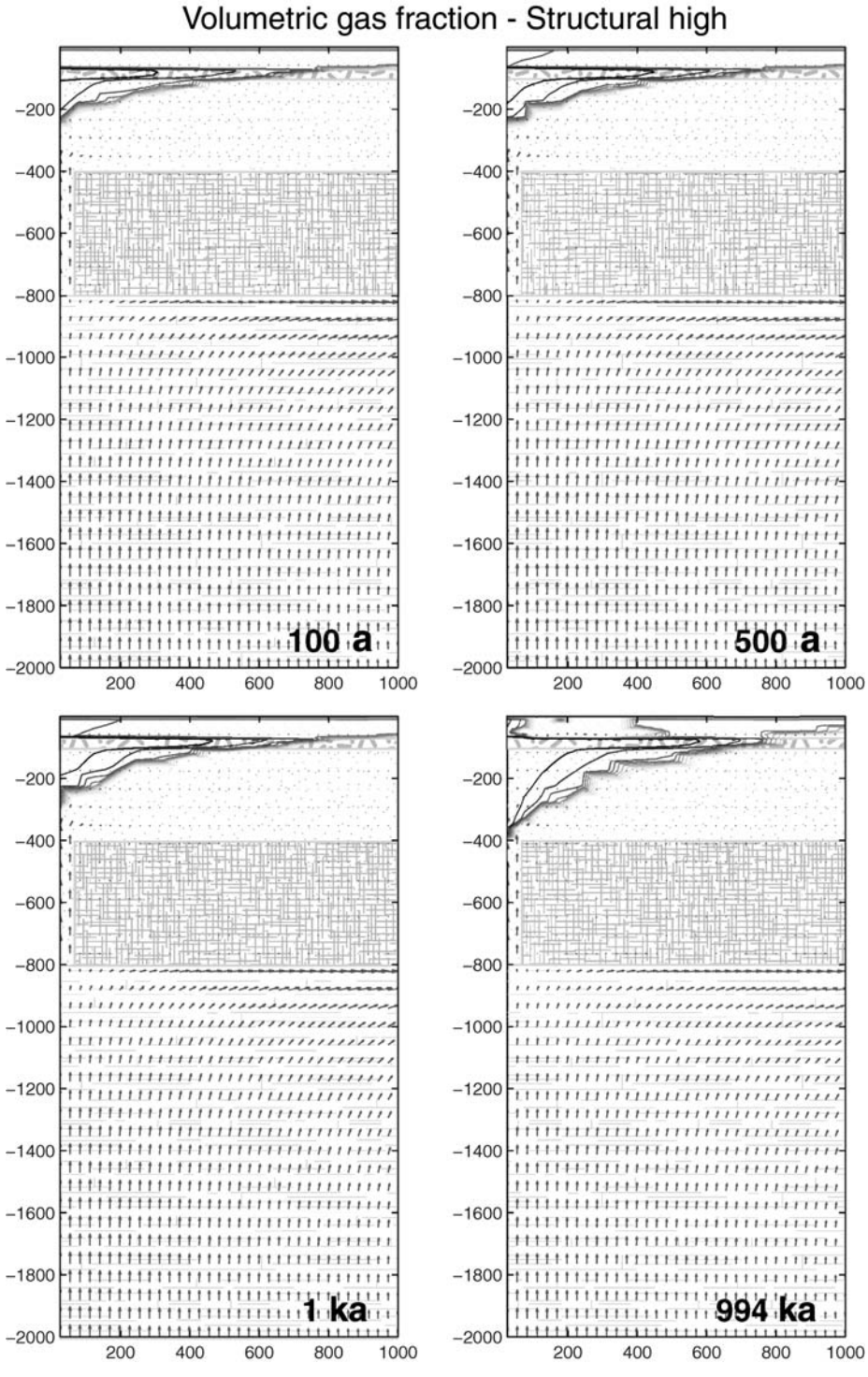

Fig. 13. Simulation 7. Volumetric gas fraction and flow pattern of liquid water at shallow depths and at different times. Contour lines are plotted every 0.005 for gas fractions ranging from 0.02 to 0.065. Maximum flow rate is 7.75×10^{-5} kg m^{-2} s^{-1}. Different patterns indicate lithologies, as shown in Figure 3, and highlight the gap through the clay layer at depth.

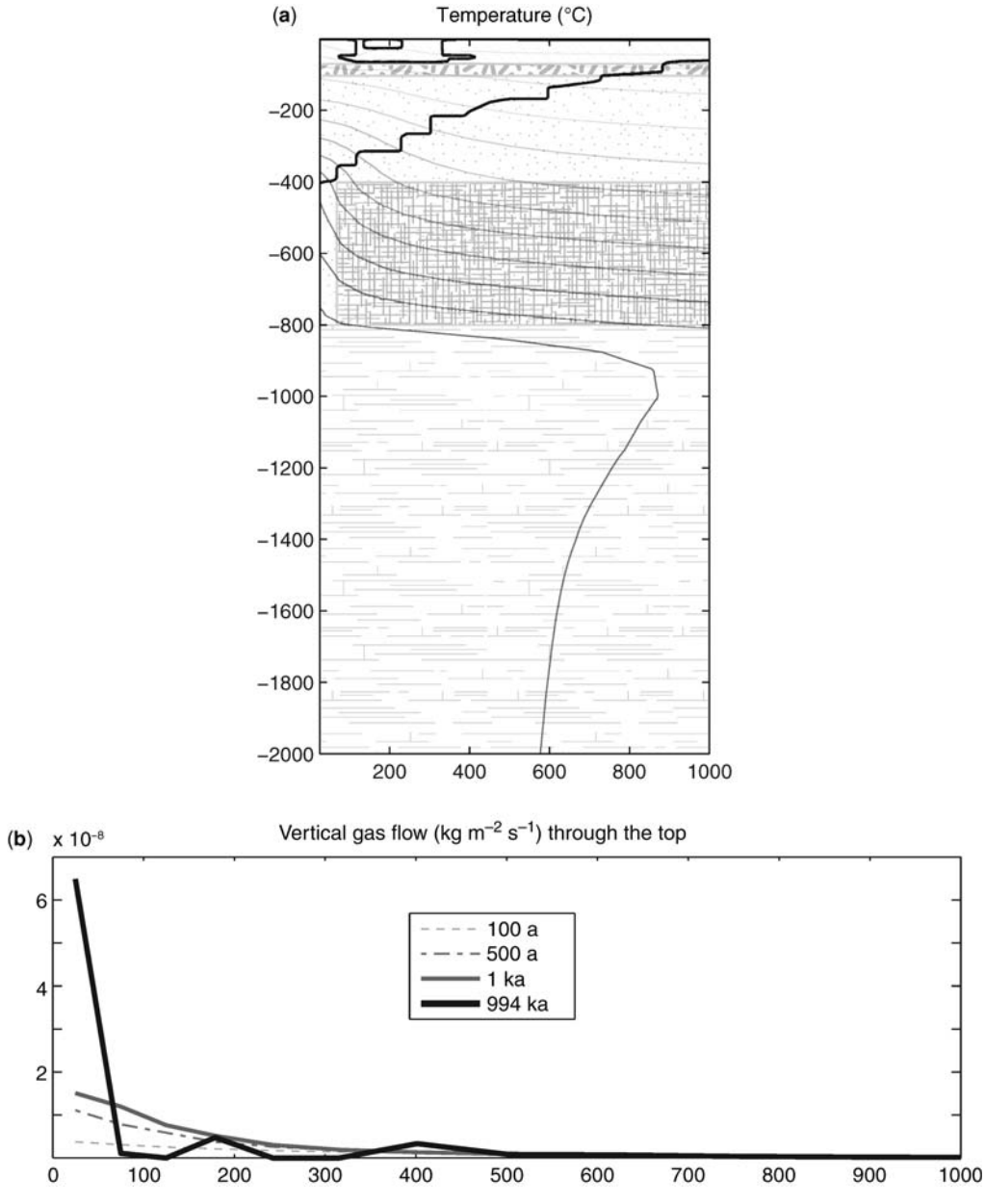

Fig. 14. Simulation 7. (**a**) Temperature (°C) distribution at the steady state. Contour lines are plotted every 10 °C, for gas fractions ranging from 30 to 140 °C. The thick, black line indicates the extent of the two-phase zone. (**b**) Gas flow rate along the surface at different times.

temperatures in the main reservoir do not necessarily relate to a lack of a heat source at depth.

Surface degassing certainly depends on the strength of the gas source at depth. A stronger input at the base reflects as a larger degassing rate at the surface (Fig. 11). Also in this case, the rate at which CO_2 is released at the surface changes with the structural setting and is larger in the case of a structural high. The stronger input also causes an enlargement of the two-phase region, and an increase of the gas fraction, especially within the less-permeable layers. For the system properties and

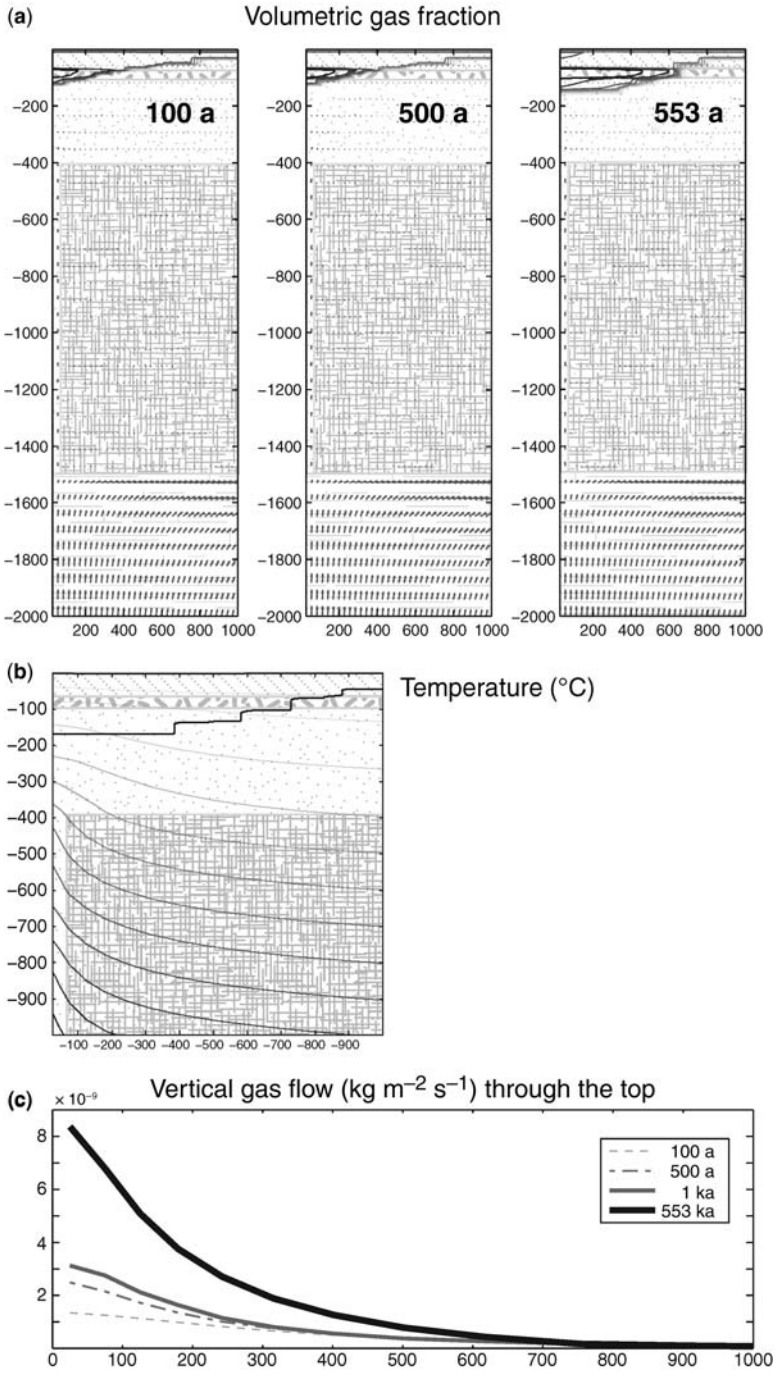

Fig. 15. Simulation 8. (**a**) Volumetric gas fraction and flow pattern of liquid water at shallow depths and at different times. Contour lines represent divisions of 0.005, from 0.02 to 0.065. Maximum flow rate for liquid water is 1.02×10^{-4} kg m^{-2} s^{-1}. Different patterns indicate different lithologies, as shown in Figure 3, and highlight the gap through the clay layer at depth. (**b**) Temperature (°C) distribution at the steady state. Contour lines are plotted every 10 °C for gas fractions ranging from 30 to 140 °C. (**c**) Gas flow rate through the surface at different times. The thick, black line indicates the extent of the two-phase zone.

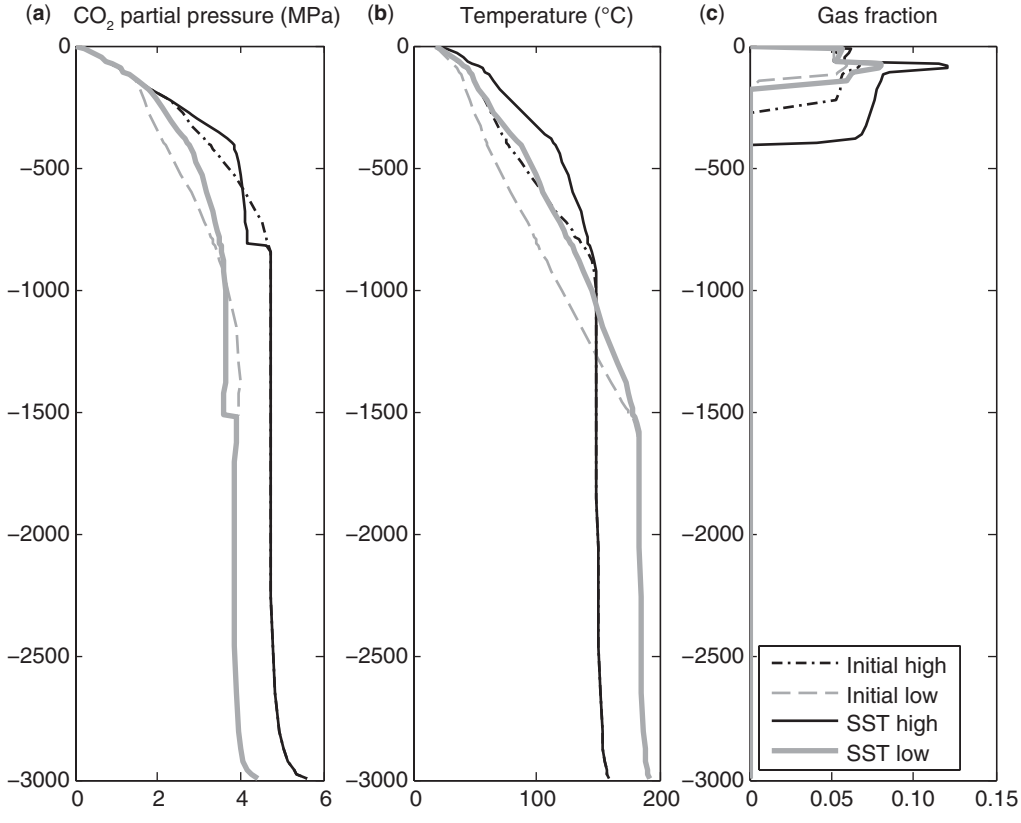

Fig. 16. Simulations 7 and 8. Distribution of CO_2 partial pressure (**a**, MPa), temperature (**b**, °C) and volumetric gas fraction (**c**) with depth, along the symmetry axis, for the cases of a structural high and low. Dashed lines indicate the vertical profiles at the beginning of the simulations (shown in Fig. 7), and solid lines indicate steady-state values.

conditions considered here, however, the maximum gas fraction achieved is always very low, and the gas phase never saturates the pore space. Slight pressurization (up to $+0.6 \times 10^5$ Pa) occurs at shallow depths (<500 m), where the gas fraction increases, for both structural settings.

Another interesting consideration arises from the simulated times. Changes imposed at the base of the domain require very long times to reach the surface (of the order of thousands of years). These times are not consistent with the occurrence of sudden changes (either in temperature or in flow rate), as have been observed at various emission points in the area. This discrepancy suggests that either these fast changes occur where local rock properties allow a faster fluid migration, or they are driven by a much shallower source, such as a change in the hydraulic properties of the cap rocks.

In our simulations, the continuity of impervious layers is a fundamental key that controls the shallow fluid circulation. A gap in the shallow pisolitic layer introduces major changes in the gas fraction and phase distribution below the surface (Fig. 12). Degassing increases by more than one order of magnitude even if the rate of CO_2 generation at depth has not changed. In our simulation, the gap in the impervious layer is filled by the underlying sand. This situation is meant to describe a damaged or fracture zone, or an impervious layer that was originally discontinuous. Drilling of a water well would actually remove the porous rock and suddenly place the gas at the well head under atmospheric pressure. This process, not simulated here, is expected to have an even larger impact on the dynamics of gas expansion and ascent, as shown by recent accidents in the area.

Our results also show that, with time, the circulation triggered by the uprising fluids culminates in flooding of the shallowest rock layer. As a result, degassing ceases where rocks become water saturated (Fig. 12). This particular phenomenon is due to the boundary conditions imposed along the top, which allow a continuous feeding of cold water at the surface. Even if not realistic, this behaviour

well illustrates the sensitivity of surface degassing to the presence of liquid water. It is reasonable to expect that drying of a shallow aquifer could result in a remarkable increase in gas emissions, which would be totally unrelated to the state of the volcano.

Finally, our results show that major effects are observed if a gap exists through the main cap rock of the reservoir at depth. Hot, CO_2-rich fluids can propagate through the clay thanks to a permeable channel-way, and freely expand within the shallow layers. As a result, not only will the emission rate at the surface increase significantly (Figs 14–16), but the temperature distribution will also be affected to shallow depths.

This result is consistent with the findings of high CO_2 partial pressure reported within the NE–SW-trending Ardea graben. This area contradicts the usual trends, in which major degassing occurs at structural highs. The Ardea graben, however, is an active tectonic area, and degassing could be associated with fracturing, which may dissect the Pliocene clay aquiclude (Faccenna *et al.* 1994).

Although preliminary, our results are consistent with the data and suggest that, upon appropriate calibration, the model could provide important insights into the mechanism controlling diffuse degassing. Future improvements should involve the simulation of complex three-dimensional domains, describing both structural highs and lows within the same simulation. Our results stress the need for a detailed definition of the rock properties and of the subsurface rock sequences, in order to define the location, size and geometry of aquicludes and permeable regions.

The integration of geophysical, volcanological, and monitoring data into a consistent physical model represents a very promising approach to both scientific and civil defence issues.

References

Amato, A. & Chiarabba, C. 1995. Earthquake occurrence and crustal structure. *In*: Trigila, R. (ed.) *The Volcano of the Alban Hills*. Tipografia SGS, Roma, 193–211.

Amato, A., Chiarabba, C., Cocco, M., Di Bona, M. & Selvaggi, G. 1994. The 1989–1990 seismic swarm in the Alban Hills volcanic area, central Italy. *Journal of Volcanology and Geothermal Research*, **61**, 225–237.

Anzidei, M. *et al.* 2008. The Albano Maar Lake high resolution bathymetry and dissolved CO_2 budget (Colli Albani volcano, Italy): Constrains to hazard evaluation. *Journal of Volcanology and Geothermal Research*, **178**, 258–268.

Barberi, F., Carapezza, M. L., Ranaldi, M. & Tarchini, L. 2007. Gas blowout from shallow boreholes at Fiumicino (Rome): induced hazard and evidence of deep CO_2 degassing on the Tyrrhenian margin of Central Italy. *Journal of Volcanological and Geothermal Research*, **165**, 17–31.

Beaubien, S. E., Ciotoli, G. & Lombardi, S. 2003. Carbon dioxide and radon gas hazard in the Alban Hills area (central Italy). *Journal of Volcanological and Geothermal Research*, **123**, 63–80.

Bianchi, I., Piana Agostinetti, N., De Gori, P. & Chiarabba, C. 2008. Deep structure of the Colli Albani volcanic district (central Italy) from receiver functions analysis. *Journal of Geophysical Research*, **113**, B09313, doi: 10.1029/2007JB005548.

Boni, C., Bono, P., Lombardi, S., Mastrorillo, L. & Percopo, C. 1995. Hydrogeology, fluid geochemistry and thermalism. *In*: Trigila, R. (ed.) *The Volcano of the Alban Hills*. Tipografia SGS, Roma, 221–242.

Capelli, G., Mazza, R. & Gazzetti, C. 2006. Strumenti e strategie per la tutela e l'uso compatibile della risorsa idrica nel Lazio: gli acquiferi vulcanici. Pitagora Editrice, Bologna, 191.

Carapezza, M. L., Badalamenti, B., Cavarra, L. & Scalzo, A. 2003. Gas hazard assessment in a densely inhabited area of Colli Albani Volcano (Cava dei Selci, Roma). *Journal of Volcanological and Geothermal Research*, **123**, 81–94.

Carapezza, M. L., Barberi, F., Tarchini, L., Ranaldi, M. & Ricci, T. 2010. Volcanic hazards of the Colli Albani. *In*: Funiciello, R. & Giordano, G. (eds) *The Colli Albani Volcano*. Geological Society, London, Special Publications of IAVCEI, **3**, 279–297.

Carapezza, M. L. & Tarchini, L. 2007. Magmatic degassing of the Alban Hills volcano (Rome, Italy): geochemical evidence from accidental gas emission from shallow pressurized aquifers. *Journal of Volcanological and Geothermal Research*, **165**, 5–16.

Chiarabba, C., Amato, A. & Delaney, P. T. 1997. Crustal structure, evolution, and volcanic unrest of the Alban Hills, central Italy. *Bulletin of Volcanology*, **59**, 161–170.

Chiodini, G. & Frondini, F. 2001. Carbon dioxide degassing from the Albani Hills volcanic region, Central Italy. *Chemical Geology*, **177**, 67–83.

Cioni, R., Guidi, M., Raco, B., Marini, L. & Gambardella, B. 2003. Water chemistry of Lake Albano (Italy). *Journal of Volcanology and Geothermal Research*, **120**, 179–195.

Conticelli, S., Boari, E. *et al.* 2010. Geochemistry, isotopes and mineral chemistry of the Colli Albani volcanic rocks: constraints on magma genesis and evolution. *In*: Funiciello, R. & Giordano, G. (eds) *The Colli Albani Volcano*. Geological Society, London, Special Publications of IAVCEI, **3**, 107–139.

Danese, E. & Mattei, M. 2010. The sedimentary substrate of the Colli Albani volcano. *In*: Funiciello, R. & Giordano, G. (eds) *The Colli Albani Volcano*. Geological Society, London, Special Publications of IAVCEI, **3**, 141–151.

De Benedetti, A. A., Funiciello, R., Giordano, G., Diano, G., Caprilli, E. & Paterne, M. 2008. Volcanology, history and myths of the Lake Albano maar (Colli Albani volcano, Italy). *In*: Cashman, K. & Giordano, G. (eds) *Volcanoes and Human History*. Journal of Volcanological and Geothermal Research, Special issue, **176**, 387–406.

Di Filippo, M. & Toro, B. 1995. *Gravity Features. In*: Trigila, R. (ed.) *The Volcano of the Alban Hills*. Tipografia SGS, Roma, 213–219.

Duchi, V., Paolieri, M. & Pizzetti, A. 1991. Geochemical study on natural gas and water discharges in the Southern Latium (Italy): circulation, evolution of fluids and geothermal potential in the region. *Journal of Volcanological and Geothermal Research*, **47**, 221–235.

ENEL 1990. Esplorazione geotermica nel P.R. Colli Albani. Internal Report, Pisa, 54.

Faccenna, C., Funiciello, R., Bruni, A., Mattei, M. & Sagnotti, L. 1994. Evolution of a transfer-related basin: the Ardea basin (Latium, central Italy). *Basin Research*, **5**, 35–46.

Funiciello, R., Giordano, G. & De Rita, D. 2003. The Albano Maar Lake (Colli Albani volcano, Italy): recent volcanic activity and evidence of pre-Roman Age catastrophic lahar events. *Journal of Volcanology and Geothermal Research*, **123**, 43–61.

Gambardella, B. *et al*. 2004. Fluxes of deep CO_2 in the volcanic areas of central-southern Italy. *Journal of Volcanology and Geothermal Research*, **136**, 31–52.

Giggenbach, W. F., Minissale, A. A. & Scandiffio, G. 1988. Isotopic and chemical assessment of geothermal potential of the Colli Albani area, Latium, Italy. *Applied Geochemistry*, **3**, 475–486.

Giordano, G. & The CARG Team 2010. Stratigraphy, volcano tectonics and evolution of the Colli Albani volcanic field. *In*: Funiciello, R. & Giordano, G. (eds) *The Colli Albani Volcano*. Geological Society, London, Special Publications of IAVCEI, **3**, 43–98.

Giordano, G., De Benedetti, A. A. *et al*. 2006. The Colli Albani mafic caldera (Roma, Italy): stratigraphy, structure and petrology. *Journal of Volcanology and Geothermal Research*, Special issue 'Explosive mafic volcanism', **155**, 49–80.

Mattei, M., Conticelli, S. & Giordano, G. 2010. The Tyrrhenian margin geological setting: from the Apennine orogeny to the K-rich volcanism. *In*: Funiciello, R. & Giordano, G. (eds) *The Colli Albani Volcano*. Geological Society, London, Special Publications of IAVCEI, **3**, 7–27.

Mazza, R. & Capelli, G. 2010. Hydrogeology of the Colli Albani volcano. *In*: Funiciello, R. & Giordano, G. (eds) *The Colli Albani Volcano*. Geological Society, London, Special Publications of IAVCEI, **3**, 189–213.

Mongelli, F., Zito, G. *et al*.1991. Geothermal regime of Italy and surrounding seas. *In*: Cermák, V. & Rybach, L. (eds) *Terrestrial Heat Flow and the Lithosphere Structure*. Springer-Verlag, Berlin/ Heidelberg, 381–394.

Pruess, K., Oldenburg, C. M. & Moridis, G. 1999. TOUGH2 User's Guide, Version 2.0, Report LBNL-43134, Lawrence Berkeley National Laboratory, Berkeley, California.

Tuccimei, P., Giordano, G. & Tedeschi, M. 2006. CO_2 release variations during the last 2000 years at the Colli Albani volcano (Roma, Italy) from speleothems studies. *Earth and Planetary Science Letters*, **243**, 449–462.

Voltaggio, M. & Spadoni, M. 2009. Mapping of H_2S fluxes from the ground using copper passive samplers: an application study at Zolforata di Pomezia degassing area. *Journal of Volcanological and Geothermal Research*, **179**, 56–68.